International Journal of Infrared and Millimeter Waves, Vol. 27, No. 4, April 2006 (© 2006)
DOI: 10.1007/s10762-006-9098-3

Terahertz time-domain attenuated total reflection spectroscopy in water and biological solution

Masaya Nagai, Hiroyuki Yada, Takashi Arikawa, and Koichiro Tanaka

Department of Physics, Graduate School of Sicience
Kyoto University
Kitashirakawa, Sakyo, Kyoto 6068502, Japan
E-mail : mnagai@scphys.kyoto-u.ac.jp

Abstract

We demonstrate time-domain attenuated total reflection spectroscopy in terahertz frequency region. Geometry of the reflection measurement is well optimized to obtain accurate optical constants of water or aqueous biomolecular system. We determine the dielectric constants of distilled water and sucrose solutions with this technique. This technique will open new aspects in the research field of biological systems in water.

Introduction

Water plays a key role for biologically functional dynamics in huge molecules. To begin with bulk water, hydrogen bonding and electrostatic interaction between molecules dominate collective motion of molecules in the timescale from hundreds femtoseconds to picoseconds, which yields various peculiar properties of water. This macroscopic motion of water is strongly distorted by bonding to huge biomolecules. Dehydration or rearrangement of hydrated water molecules in the timescale from picoseconds to nanoseconds brings about macroscopic structural transformation of biomolecules [1-3]. For distinguishing these macroscopic motions, it is crucial to understand the response function of water in the microwave and far-infrared region. Thus the exact recognition of bulk water itself and the technique to detect tiny perturbation of response function by solute molecules are required. The progress of these researches have been made and numerous experimental and theoretical studies in microwave region have been published [4-6].

Dielectric properties in the far-infrared region have also been investigated with Fourier transform spectroscopy [7]. In particular, remarkable development of ultrashort light beams technique promotes terahertz time-domain spectroscopy (THz-TDS) [8], facilitating the measurements of dielectric constants. In this experimental technique, temporal profile of electric field is detected with optical sampling technique, giving optical constants of a sample directly without

Kramers-Kronig relations. In the reflection geometry, which is useful for samples with strong absorption such as polar liquids, and hydrated biomolecules, Fourier transforms of the incident and reflected electric field (E_{in} and E_r) yield Fresnel reflection coefficient at the boundary, deriving the complex dielectric constants [9-12].

Recently we proposed a novel TDS with attenuated total reflection (ATR) technique [13], which can be used to access samples with various shapes and optical properties. In general, ATR technique provides information on the interaction between the sample and the evanescent wave traveling along a prism surface. In ATR geometry, the electric field at the boundary is the largest due to instructive interaction between incident and reflected electric field, enhancing the interaction between light and materials. Harrick approximated the attenuation of reflectivity as a linear function of the sample's absorption and described the interaction of evanescent wave as the effective penetration thickness [14]. This indicates that observed attenuation of reflectivity is nearly equivalent to the transmission spectrum. In TDS, the phase shift is also sensitive to small change of optical constants as well as reflectivity. Graphical representation of optical constant on complex reflective coefficient plane indicates that *p*-polarized ATR geometry is the most useful in the time-domain (TD) reflection measurements to determine optical constants of a sample exactly [15]. In this report, we demonstrate the availability of determination of dielectric constant of distilled water and the solution with TD-ATR technique.

Experimental Setup

We use optical pulses from a fiber laser (IMRA) with a repetition rate of 50MHz, an average power of 20 mW, center of frequency of 780 nm, and pulse duration of 90 fs (full-width at half-maximum-intensity), which is split into two beams. One of the beams is focused on the photo-conductive antenna to generate coherent THz pulses. The emitted THz pulses are focused onto the (110) oriented-ZnTe crystal surface with the thickness of 2 mm using four off-axis parabolic mirrors. The other beam is used as a sampling beam of the transmitted THz pulses, and are also focused onto the same spot of the ZnTe crystal for the detection through the small hole of a parabolic mirror, and the birefringence of the sampling beams induced by the electric field of THz pulses are measured using a quarter wave plate, Wolston prism, and two balanced-Si-photo-detectors. To improve signal-noise ratio, vias voltage applied to the photo-conduction antenna is modulated at 80 kHz, and modulated EO signals are detected using a lock-in amplifier. By changing the time delay between the two pulses, the electric field amplitude of THz pulses can be detected as a function of time.

Experimental setup is basically conventional TDS system in transmission geometry [13]. We easily realize ATR geometry by setting a Si Dove prism at the focus point of THz pulse as shown in Fig. 1. Since remarkable feature of Dove prism is the same direction of incident and outgoing beams, the insertion of this prism does not influence the optical pathway of transmission geometry. We simply design a Dove prism with the side view of an isosceles triangle. If

incidence angle for total internal reflection at the bottom plane is defined as θ, apex angle of prism is 2θ. Assuming that incident beam in the direction parallel to the bottom plane is entering into the center on a side slope of prism, corresponding incident angle into a prism is also θ. Thus apex angle of prism 2θ should be satisfied with the relation of $\sin\theta = n_1 \sin(2\theta - \pi/2)$, deviated from Snell's law and geometrical configuration. In the case of Si Dove prism with index of n_1=3.42, the incident angle should be θ =51.6º. This incident angle indicates that total reflection condition is satisfied for the sample with refractive index of n_1<2.68. Since Dove prism is designed for parallel or collimated incident beam, optical path length through the prism should be less than confocal length of focused THz beam in the transmission geometry [16].

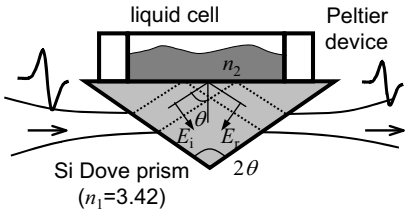

Fig.1: The sketch of TD-ATR geometry using Dove prism

The liquid sample is put in the cell touching on the ATR prism. This cell is attached to a 30 W Peltier electric device for temperature control from 253 to 353 K. In the measurements of temperature dependence, we have to concern about the thermal expansion and temperature dependence of the refractive index n_1 of the Dove prism. It does not strongly influence the incidence condition, but change of the optical path length causes phase shift of THz pulse. Actually the temporal profile of electric field without sample linearly shifts 6 fs by the temperature of 1 K changed. Thus we carefully measure electric field of reference whenever the temperature of water sample is changed.

TD-ATR measurements in distilled water

Figure 2 (a) shows the temporal profile of the electric field in ATR geometry with *p*-polarized incidence. Upper curve E'_r is measured without sample, which can be considered as the total-reflected pulse on the prism surface. Lower curve E_r is measured with the distilled water sample on the prism surface at temperature of 293 K. One can see that amplitude of the electric field is reduced with its position slightly delayed (~0.1 ps). Fourier transforms of temporal profile yield both amplitude and phase of electric filed in the frequency domain. We obtain the attenuated total reflectivity $ATR = |E_r(\omega)/E'_r(\omega)|^2$ and relative phase shift $\Delta\phi = Arg[E_r(\omega)] - Arg[E'_r(\omega)]$ from experimental results. Figure 2 (b) shows ATR and $\Delta\phi$ derived by the temporal profiles in Fig. 2 (a).

This observed complex value of E_r/E'_r corresponds to the ratio of Fresnel coefficients $E_r/E'_r = (E_r/E_{in})(E_{in}/E'_r) = r/r'$. Assuming incidence from the medium

with the index of $n_1$to the medium with the index of n_2 with the angle of θ, Fresnel reflective coefficient for *p*-polarized incidence is expressed as the following,

$$r^p = \frac{n_1\sqrt{1-(n_1/n_2)^2\sin^2\theta} - n_2\cos\theta}{n_1\sqrt{1-(n_1/n_2)^2\sin^2\theta} + n_2\cos\theta}. \quad (1)$$

In the case of Si Dove prism, Fresnel coefficient of reference beam (n_2=1) is the given constant value of r' = exp(i 0.15), and Fresnel constant of r is the function of n_2. Thus we easily obtain two solutions $\varepsilon_{2\pm}$= n_2^2 = $(B\pm(B^2-AB\sin^2(2\theta))^{1/2})/(2A\cos^2\theta)$ from eq. (1), where $A=(r-1)^2$ and $B=(r+1)^2$. Due to the causality we should chose the solution with positive imaginary part as the dielectric constant ε_2, as shown in Fig. 3 (a).

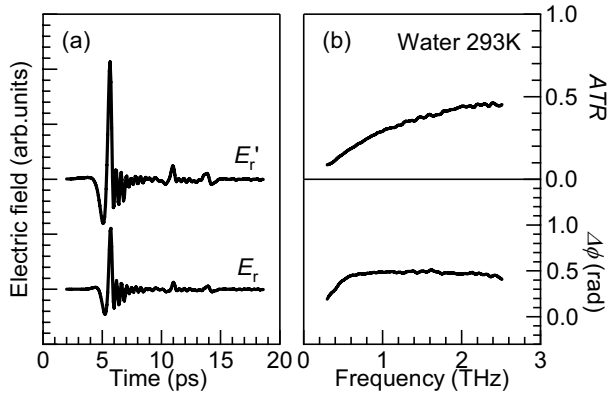

Fig.2 (a): The temporal profiles of electric field in *p*-polarized ATR geometry without sample and with the distilled water sample on the prism surface. (b) Corresponding ATR and relative phase spectra.

ATR geometry with an adequate incident angle has an potential for exact determination of dielectric constants. It is because reflective coefficient is sensitively changed by small change of sample's optical constant. For its demonstration, we plot dispersion curves on the complex plane of refractive coefficient [15] denoted by A in Fig. 3 (b). The length from the original point and the polar angle corresponds to amplitude of Fresnel coefficient $|r|$ and phase Arg[r], just equivalent to $\sqrt{ATR}$ and $\Delta\phi$+0.15 in Fig. 2 (b), respectively. We also add the dispersion of water for reflection in normal incidence. The curves denoted by B and C show the Fresnel coefficient for normal incidence from vacuum and Si window, respectively. They are located in the narrow region of lower half complex plane. However, with increase of incident angle, the dispersion expands with moving towards upper half of complex plane. This implies that reflective coefficient is sensitively change by small change of sample's optical constant. To put it the other way round, the uncertainty of

amplitude and/or phase shift of the measured reflective coefficient, for example, due to the fluctuation of the laser power or uncertainty of optical path length does not strongly influence the errors of dielectric constant. Error bars in Fig. 3 (a) show that transformed uncertainties of dielectric constants of water at 2.0 THz, where constant uncertainty of the reflective coefficient is assumed as $|\Delta r| = 0.02$. This indicates that ATR geometry denoted by A is adaptable for exact determination of optical constants in water.

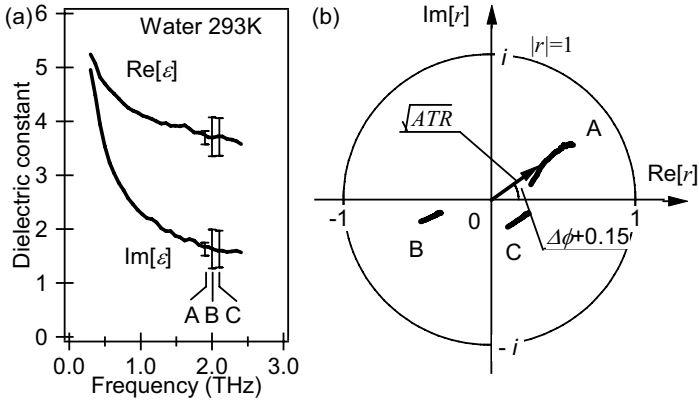

Fig.3 (a): Dielectric constants of distilled water at 293 K measured by THz TD-ATR method. (b) Complex reflective coefficients of water for various geometries. Prism index and incident angle are (A) $n_1 = 3.42$ and $\theta = 51.6^{\circ}$, (B) $n_1 = 1$ and $\theta = 0^{\circ}$, (C) $n_1 = 3.42$ and $\theta = 0^{\circ}$. We also add the evaluated errors of the dielectric constant at 2 THz in Fig. (a) in each geometry assuming given uncertainty of reflective coefficient $|\Delta r| = 0.02$.

Temperature dependence of dielectric constants of distilled water

Figure 4 shows the real and imaginary parts of complex dielectric constants in distilled liquid water and ice at different temperatures. In liquid water, both real and imaginary part increase in the low frequency region. The magnitude of the imaginary part decreases gradually with decreasing temperature, and even below the melting point (273 K), one can see continuous decreasing (supercooled state). With a physical perturbation to the water in the super-cooled state, one can easily induce freezing. The imaginary part suddenly falls down to nearly zero after freezing. In ice, there remains a small component that increases with increasing frequency. The origin of the residual component in ice is attributed to disorder-induced transition between different translational vibration modes [17].

Rønne et al. determined dielectric constants of water in the frequency range between 0.1 and 2.0 THz in the temperature range between 270 and 368K with THz-TDS in the reflection geometry [10-12]. Our experimental results are

slightly smaller than their evaluations. However, our evaluation is in good agreements with the results obtained by the reflection depressive Fourier transform spectroscopy [7]

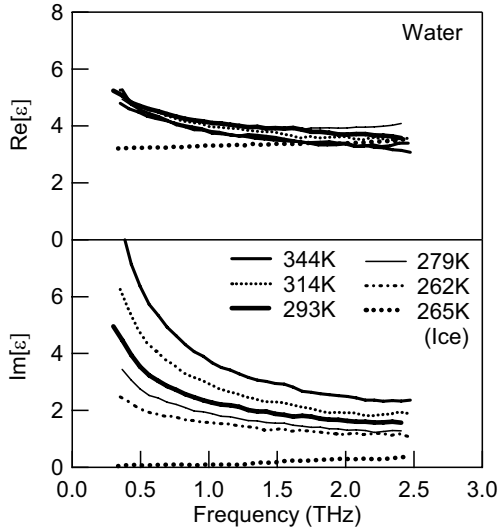

Fig. 4 Real (upper) and imaginary (lower) part of complex dielectric constant of liquid water and ice at different temperatures.

Several researchers have pointed out that relaxation response of water has two components with relaxation time of several tens picoseconds and femtoseconds. Slower component, originating from rotational relaxation, has been intensively investigated with dielectric measurements in the microwave frequency region [4,5,18]. Faster component is expected to lie in the THz frequency region, but its characters have not been clarified. Rønne claimed that their experimental results obtained with THz-TDS were well reproduced by a conventional double Debye relaxation model [10-12]. However, the analysis with the assumption of only two relaxators is inadequate to assess the dielectric dispersion in the THz region, because many vibrational modes in the high frequency region should contribute to the dielectric dispersion of water in the THz frequency region. Actually, lower-frequency tail of the mode around 200 cm^{-1}, originating from the translational modes arising from the stretching of hydration bonding [7], influences the dispersion at 2 THz. Thus dielectric constant should be described by the following relation,

$$\tilde{\varepsilon}(\omega) = \varepsilon_\infty + \frac{\varepsilon_s - \varepsilon_1}{1 + i\omega\tau_D} + \frac{\varepsilon_1 - \varepsilon_\infty}{1 + i\omega\tau_2} + \frac{A}{\omega_T^2 - \omega^2 + i\omega\gamma}, \qquad (2)$$

where τ_D and ε_s - ε_1 are the relaxation time and the strength of the rotational Debye relaxator, and τ_2 and ε_1 -ε_∞ are those of the second Debye relaxator, respectively. The fourth term corresponds to the dispersion due to translational mode.

In order to focus on the femtoseconds component, we remove the other contributions from the dielectric constants. We assume the contribution of the slow rotational relaxation component evaluated from the GHz region experiment [4,5,18], and also assume the high-frequency Lorentz oscillator evaluated from the IR measurements [7]. The parameters of these two components at 20 ºC are τ_D= 9.36 ps, ε_s = 80.2, ε_∞ = 2.5, ω_T = 5.6 THz, $\gamma/2\pi$ = 5.9 THz, and A =38 THz^2, respectively.

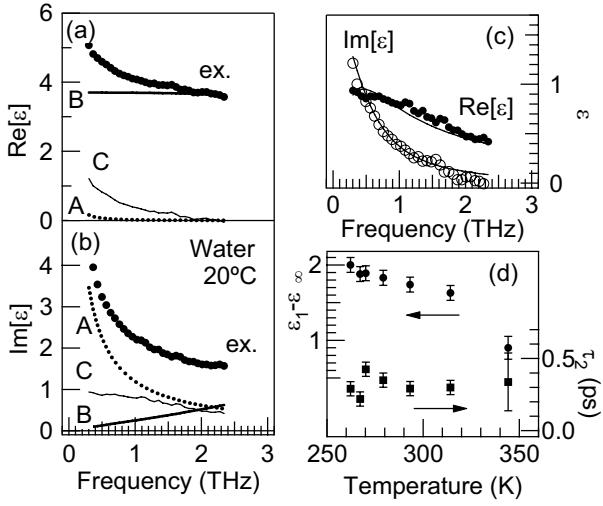

Fig. 5 (a,b) Dielectric constants of water at the temperature of 20 ºC (closed circles). The curves denoted by A-C correspond to the rotational relaxation component with τ_D, translational mode with ω_0 including ε_∞, and component obtained by subtracting these components, respectively. (c) the femtoseconds component corresponding to C in Figs. 5 (a) and (b) (closed and open circles) and the best fitted curve to the Debye relaxation (solid curves). (d) Temperature dependence of fitted τ_2 and ε_1 -ε_∞.

In this way, the spectra shown in Fig. 5 (c) are obtained by subtracting these two components. Left graph shows the contribution of each component. One can see that the contributions of three components to dielectric constant in THz frequency region are almost the same. The detail of the residual component is shown in Figs. 5 (a) and 5 (b), both real and imaginary parts in dielectric constants decreases with frequency. We analyze these spectra with Debye-type dispersion to find the characteristic properties. Best-fitted parameters are τ_2 = 0.30 ps and ε_1 = 5.3. These theoretical curves reproduce the experimental results more excellently than those obtained with double Debye model. Evaluated relaxation time is longer than those evaluated with double Debye model (0.17 ps) used by Rønne et al. [9]. Fitting parameters of τ_2 and ε_1 -ε_∞ are summarized in Fig. 5 (d). These time constants are different from that evaluated from Raman

spectroscopy or Kerr effect spectroscopy [19,20]. In the case of isotropic liquid system, it has been considered not necessary to coincide the behavior of dipole evaluated from infrared spectroscopy with that evaluated from Raman spectroscopy.

Dielectric properties of water near the critical point [21] give us one interpretation of the THz component. Since the dielectric relaxation of water in the dilute and gaseous region is dominated by the binary collision of water molecules, the relaxation time should be equal to the collision time. This time constant is inversely proportional to the density of water molecule and the square root of temperature. Thus collision time at the density of liquid become shortened as short as subpicoseconds. Alternatively, librational motion of water molecules incorporated in the hydrogen-bond network is dominant in dense liquid region, causing slower Debye relaxation, and these relaxation components are competitive near the critical point. Therefore we may attribute the THz component to the collision limited relaxation processes. This interpretation is supported by the experimental results that τ_2 is less dependent on the temperature than τ_D. The evaluation of the vibrational mode strongly influence on the analysis of τ_2 components. In particular, spectral lineshape of transnational mode becomes ambiguous with high temperature. For further verifying the nature of the THz component, precise determinations of dielectric constants in the wide frequency region under various temperature, and pressure are decisive.

Dielectric properties of sucrose solution

As mentioned above, we demonstrate that THz TD-ATR spectroscopy allows us to determine exactly the dielectric constant of distilled water. It implies that this technique is available to distinguish the slightly perturbed response function by dilute biological molecules dissolved in water. Figure 6 shows the dielectric constant of water (bold curves) and sucrose solutions (thin curves). The concentration of the solutions are 0.15, 0.31, 0.63, and 0.99 mol/*l*, respectively. We also deduce the optical constants of sucrose crystal as dashed curves shown in Fig. 6, indicating that the spectra of sucrose solutions have completely different characteristics from that of the crystal. Although one can see characteristic sharp absorption line at 1.45 THz in sucrose crystal originating from the intermolecular vibration mode, the spectral lineshape in solution is more like that of water. Roughly speaking, imaginary part of ε in the solution is reduced with increasing the concentration of the solution. This is because water molecules are partially replaced with sucrose molecules with small susceptibility.

However, Fig. 6 indicates that the change of the dispersion curves of solution induced by solute molecules strongly depends on the frequency. Inset shows the concentration dependence of Im[ε] at 1.5 THz. Dielectric constant decreases with concentration in dilute solution region, but it increases in the dense region. This indicates that the dielectric constant cannot be simply expressed as a linear function of concentration.

In general, the dispersion of the solution can be described by a weighted sum of polarizabilities of solute and solvent, taking into account the local field effect.

In the simplest case polarizability of each component can be expressed with the Clausius-Mossotti relation [22]. Refractive index of sucrose solution in the visible region can be successfully described with considering Lorentz's local field. We also analyzed our experimental results with the Clausius-Mossotti relation, but our experimental results cannot be reproduced completely. Since orientational relaxation is dominant in dielectric properties in the THz frequency region, the analysis including permanent dipole of water molecule is essential [23]. Thus cautious analysis including various predicted effects is required for clarifying the macroscopic motions of water and solute molecules.

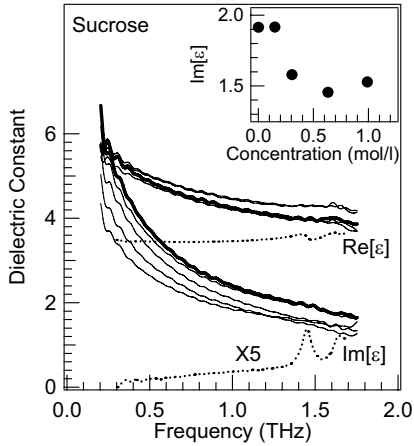

Fig. 6 The dielectric constants of water (bold curves) and sucrose solution (thin curves). The concentration of solution are 0.15, 0.31, 0.63, and 0.99 mol/*l*, respectively. Dashed curves show the dielectric constants of sucrose crystal. Inset shows the concentration dependence of imaginary part of dielectric constant at 1.5 THz.

Conclusions

In summary, we demonstrate the exact determination of dielectric constant of distilled water and sucrose solution with TD-ATR technique. This geometry allows us to determine dielectric constants more exactly than that in normal incidence. This technique has also an advantage that sample preparation for this technique is minimal compared to the troublesome fabrication of thin film, transparent pellet with dilute sample, and specific liquid cell for transmission measurement, allowing repetitive measurements of the various samples. This technique will be applicapable to measure various dilute and aqueous biological systems.

Acknowledgments

This work is supported by the SCOPE program from the Ministry of Public

Management, Home Affairs, Posts, and Telecommunications, Japan, and the Grant-in-Aid for the 21st Century COE "Center for Diversity and Universality in Physics" from the Ministry of Education, Culture, Sports, Science and Technology (MEXT) of Japan. Authors also acknowledge Grant-in-Aid for Scientific Research (A) (No. 17204024) of Japan Society for the promotion of Science for financial support. The authors are grateful to H, Ohtake, T. Hirosumi, M. Yoshida, and S. Saito for their technical supports.

References

1. G. Otting, E. Liepinsh, K. Wuthrich, “Protein hydration in aqueous-solution“, Science, **254**, 974 (1991).
2. S. K. Pal and A. H. Zewail, “Dynamics of Water in Biological Recognition”, Chem. Rev., **104**, 2099 (2004).
3. S. Mashimo, S. Kuwabara S. Yagihara, K. Higasi, “Dielectric relaxation time and structure of bound water in biological materials” J. Phys. Chem. **91**, 6337 (1987).
4. R. J. Speedy and C. A. Angell, “Isothermal compressibility of supercooled water and evidence for a thermodynamic singularity at –45°C”, J. Chem. Phys. **65**, 851 (1976).
5. U. Kaatze, “Complex permittivity of water as a function of frequency and temperature”, J. Chem. Eng. Date, **34**, 371 (1989).
6. Y. Z. Wei, A. C. Kumbharkhane, M. Sadeghi, J. T. Sage, W. D. Tian, P. M. Champion, S. Sridhar, M. J. Mcdonald, “Protein hydration investigations with high-frequency dielectric-spectroscopy”, J. Phys. Chem. **98**, 6644 (1994).
7. M. N. Afsar and J. B. Hasted, “Measurements of optical-constants of liquid H_2O and D_2O between 6 and 450 cm^{-1}”, J. Opt. Soc. Am. **67** 902 (1977).
8. *Terahertz Optoelectronics*, ed. by K. Sakai, (Springer, Berlin, 2005).
9. L. Thrane, R. H. Jacobsen, P. U. Jepsen, and S. R. Keiding, “THz reflection spectroscopy of liquid water”, Chem. Phys. Lett. **240**, 330 (1995).
10. C. Rønne, L. Thrane, P. Åstrand, A. Wallqvist, K. V. Mikkelsen and S. R. Keiding, “Investigation of the temperature dependence of dielectric relaxation In liquid water by THz reflection spectroscopy and molecular dynamics simulation”, J. Chem. Phys. **107**, 5319 (1997).
11. C. Rønne, P. Åstrand, and S. R. Keideing, “THz Spectroscopy of Liquid H_2O and D_2O”, Phys. Rev. Lett. **82**, 2888 (1999).
12. C. Rønne and S. R. Keiding, J. Mol. Liq. **101**, 199 (2002).
13. H. Hirori, K. Yamashita, M. Nagai and K. Tanaka, “Attenuated Total Reflection Spectroscopy in Time Domain Using Terahertz Coherent Pulses”, Jpn. J. Appl. Phys. **43,** L1287 (2004).
14. N. J. Harrick, *Internal Reflection Spectroscopy*, Interscience, (1967).
15. M. Nagai, H. Yada, T. Arikawa, H. Hirori, and K. Tanaka, “Smith chart analysis for optimized determination of optical constants in terahertz time-

domain reflection spectroscopy", submitted.
16. A. Yariv, *Quantum Electronics* 3rd ed. (Willey, New York,1989).
17. O. Mishima, D. D. Klug, and E. Whalley, "The far-infrared spectrum of ice Ih in the range 8–25 cm^{-1}. Sound waves and difference bands, with application to Saturn's rings", J. Chem. Phys. **78,** 6399 (1983).
18. R. Bchner, J. Barthel and J .Stauber, "The dielectric relaxation of water between 0 ºC and 35 ºC", Chem. Phys. Lett. **306** (1999) 57.
19. K. Mizoguchi, T. Ujike, and Y. Tominaga, "Dynamical structure of water in NaCl aqueous solution", J. Chem. Phys. **109**, 1867 (1998).
20. E. W. Castner, Jr. and Y. J. Chang, Y. C. Chu and G. E. Walrafen, "The intermolecular dynamics of liquid water", J. Chem. Phys. **102**, 653 (1995).
21. K. Okada, M. Yao, Y. Hiejima, H. Kohno, and Y. Kajihara, "Dielectric relaxation of water and heavy water in the whole fluid phase", J. Chem. Phys. **110**, 3026 (1999).
22. R. P. Feynman, *The Feynman Lectures on Physics* ,Vol.2, Chap.11 (Redwood, Addison- Wesley,1989).
23. T. Arikawa, M. Nagai, and K. Tanaka, "A novel method to evaluate whole number of hydrated water molecules by THz time-domain attenuated total reflection technique" Extended abstract in International Workshop on Terahertz Technology, 17PS-30 (Osaka, 2005).